ELSEVIER

October 1995

Optical Materials 4 (1995) 741–755

OPTICAL Materials

High quality ZnO layers with adjustable refractive indices for integrated optics applications

R.G. Heideman, P.V. Lambeck, J.G.E. Gardeniers

MESA Research Institute, University of Twente, P.O. Box 217, NL-7500 AE Enschede, The Netherlands

Received 15 March 1995; revised 19 May 1995; accepted 15 June 1995

Abstract

Thin (~ 1 μm) crystalline ZnO films with a good optical quality and a good (0002) texture are grown under two considerably different process parameter sets using a r.f. planar magnetron sputtering unit. The optical parameters of the two corresponding ZnO layers are distinctly different: high refractive index (≅ 2.0 at λ = 632.8 nm) ZnO films resembling the single crystal form, and ZnO films with considerably lower (typical difference 0.05) refractive indices. The refractive index of the latter ZnO layers is adjustable (~ 1.93–1.96 at λ = 632.8 nm) through the process deposition parameters. It is shown that the difference in refractive index between the two ZnO types most probably results from a difference in package density of the crystal columns. The optical waveguide losses of both ZnO types are typically 1–3 dB/cm at λ = 632.8 nm, however the low refractive index ZnO layers need a post-deposition anneal step to obtain these values. The two ZnO types are used to fabricate optical channel- and slab waveguides with small refractive index differences.

1. Introduction

Zinc oxide (ZnO) offers many possibilities when used in thin film technology. It can easily be deposited at moderate temperatures on several substrates including silicon. Its (relatively large) electro-mechanical properties makes it particularly useful in surface acoustic wave (SAW) devices [1,2] and micro mechanics [3,4]. Furthermore because of its transparency for wavelengths between 400 nm and (at least) 2 μm and its electro-optical and elasto-optical properties, ZnO is an interesting material for application in integrated optical devices. Use of silicon wafers as substrates for the integrated optical thin film system provides the possibility of monolithic integration of acoustic devices with integrated optics (IO) and electronics, that is missing in the generally applied $LiNbO_3$ acousto-optical devices [5,6]. Despite this device flexibility, ZnO has only little applications in the integrated optics field. A reason for this could be the relatively large attenuation values for optical modes in (sputtered) ZnO layers, which are typically 1 dB/cm [7,8]: however, it is possible to strongly reduce this by laser annealing [9] to values as low as 0.01 dB/cm. More important could be the difficulties in the fabrication of single-mode waveguides in ZnO, which is caused by the high refractive index contrast between ZnO and the most often used substrate material, silicon dioxide (SiO_2). This large index difference does not only require small channel dimensions, but also leads to optical mode field distributions which are not compatible with that of a standard single mode fiber. This results in a very low efficiency of the transfer from fibers to the IO system.

For improving this fiber to chip coupling higher refractive index materials should be applied as cover and substrate layers. In general, this strongly degrades

0925-3467/95/$09.50 © 1995 Elsevier Science B.V. All rights reserved
SSDI 0925-3467(95)00028-3

the effects of the electro-optical and acousto-optical properties of the IO system however. This dilemma can be solved if ZnO films with different values of refractive index could be obtained. We found that this could be achieved by varying the process parameters of the planar magnetron sputtering process used for the deposition of the ZnO layers. The deposition process is optimized with respect to the boundary conditions stemming from the IO application, i.e. low optical attenuation and good thickness uniformity. Finally we were able to determine two parameter sets: one in which the optical parameters of the ZnO layer resemble those of single crystals (refractive indices at wavelength $\lambda = 632.8$ nm approximately 2.00), and one in which the refractive indices are much lower and even adjustable to a certain extent (1.93 to 1.96). For obtaining more knowledge about the origin of these refractive index differences, the two types of ZnO are then studied in more detail using refractive index dispersion measurements, transmission spectroscopy, X-ray diffraction (XRD), scanning electron microscopy (SEM) and transmission electron microscopy (TEM). From these characterization methods conclusions will be drawn upon the crystallinity of the ZnO films and the nature of the differences (a difference in package density) between them. Finally several applications combining the two ZnO types will be discussed.

2. Experimental

2.1. Sputter deposition of ZnO

The ZnO layers were deposited on thermally oxidized monocrystalline silicon wafers (Wacker, 3 inch diameter, thickness 0.4 mm) and quartz (suprasil, 1 inch diameter, thickness 1 mm) as substrate material. The oxidition occurs in water vapour using a conventional resistance heated furnace set at a temperature of 1150°C for 800 minutes, resulting in a 2 μm thick SiO_2 layer.

We deposited our ZnO films using a r.f. planar magnetron sputter unit [8]. The metallic Zn target (99.999%) with a diameter of 6 inch is reactively sputtered using 99.999% pure oxygen (O_2). The residual gas pressure before sputtering is about 3×10^{-5} Pa. The oxygen pressure P_{O_2} during sputtering can be varied between 0.5 Pa and 10 Pa. The substrate is clamped in a substrate holder which is placed above the target at a distance $d_{t\text{-}s}$. This distance can be varied between 3 and 10 cm. The substrate holder and therefore also the substrate can be heated by means of an ohmic coil to temperature T_s which is varied between 125 and 590°C. The applied r.f. power P_{RF}, which is coupled to the target by means of a manually operated matching network, can be varied between 600 and 1800 Watt. All four mentioned process parameters (P_{O_2}, $d_{t\text{-}s}$, T_s and P_{RF}) were varied in the experiments.

After removal from the vacuum chamber, it is possible to give the wafers an additional annealing step [10]. This post-deposition anneal step is done in ambient atmosphere in a resistance heated oven, at a temperature of 400 and/or 450°C.

2.2. Characterization

The structural properties of ZnO strongly determine the optical (as well as the electrical) properties of the ZnO films [11]. By checking the optical characteristics of the films, a qualitative impression of the ZnO layers can therefore be obtained. A quick impression of uniformity of the ZnO films can be obtained from ellipsometry (apparatus: Plasmos). More accurate data on thickness and refractive index are derived by using the prism coupling method [12] applying a rutile prism. In this way also the refractive index dispersion can be measured, using more wavelengths. Using the Kramers–Kronig relations, this can also be calculated from the transmission spectrum of the layers. This transmission is measured (apparatus: Shimadzu) in the range of 190 nm to 3200 nm, using the quartz as substrate.

It should be noted that besides the refractive indices also the ZnO waveguide optical losses vary with wavelength, mainly due to the intrinsic absorption of ZnO (see Section 3.2) and to the reduction of the effects of light scattering at larger wavelengths. For measuring the optical losses of the films acting as the slab waveguides both the "eye sensitivity rule" (for determining the higher attenuation values) and the scanning photodiode method are used [13,14].

To obtain a more detailed impression of the effects of sputter-deposition parameters and post-deposition annealing on the structural properties of the ZnO films, we performed X-ray diffraction measurements on several of the available samples. With XRD it is possible to obtain information on crystallographic symmetry,

texture and strain (both residual- (macro-) and micro strain). The apparatus (Philips) uses a copper (Cu) source ($\lambda_{K_{\alpha 1}}=0.15406$ nm, ($\lambda_{K_{\alpha 2}}=0.154439$ nm) with a Ni-filter. By using θ–2θ scans the crystallographic symmetry can be determined. The texture of the films is revealed by using both the θ–2θ scans and the rocking curves (θ-scan at fixed 2θ value). While comparing the peak position in the θ–2θ scan with that of a perfect crystal, the residual strain in the layers can be determined, while local lattice distortions (micro-strain) can be calculated from the line-broadening of this scan.

Structural information can also obtained with scanning and transmission electron microscopy (SEM and TEM, respectively). Furthermore, with SEM it is possible to obtain additional details about film structure such as surface roughness, initial layer information, and the dimensions of the ZnO columns. Even smaller details such as (ir)regularities of the crystal and its columnar boundaries can be made visible using TEM.

3. Results and discussion

3.1. Thickness uniformity

As the thickness uniformity with fixed dimensions is mainly determined by the distance between target and substrate $d_{t\text{-}s}$, this was the first parameter to be optimized. Because the centres of the target and the substrate were aligned, it is expected that the thickness distribution across a wafer should be circularly symmetric. Therefore the non-uniformity can be defined as the one dimensional deviation of the thickness normalized to the layer thickness in the center of the wafer. In Fig. 1 the most important results are presented.

From Fig. 1a it can be concluded that the best uniformities are obtained at the $d_{t\text{-}s}$ values of 10 cm (with a circular symmetric gaussian profile) and 3.5 cm (a ring-shaped profile which is shifted with respect to the center of the wafer). The latter optimum is in good agreement with theory [14]: a uniform thickness dis-

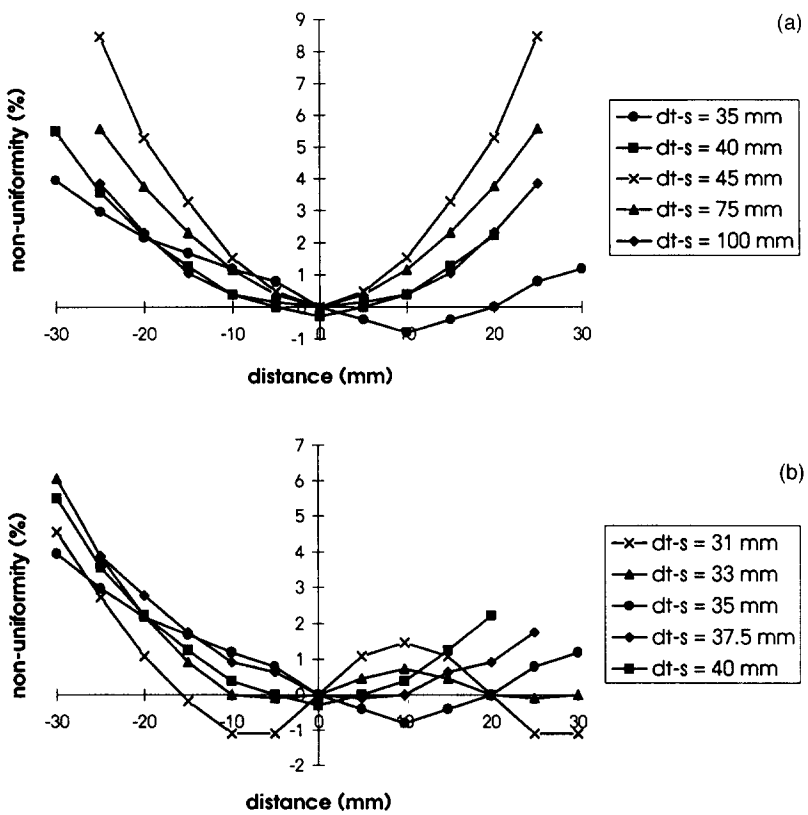

Fig. 1. Thickness non-uniformity as a function of the distance to the center of the wafer, with the target-substrate distance $d_{t\text{-}s}$ (in mm) as parameter (a). The non-uniformity around the $d_{t\text{-}s}$ value of 35 mm (b).

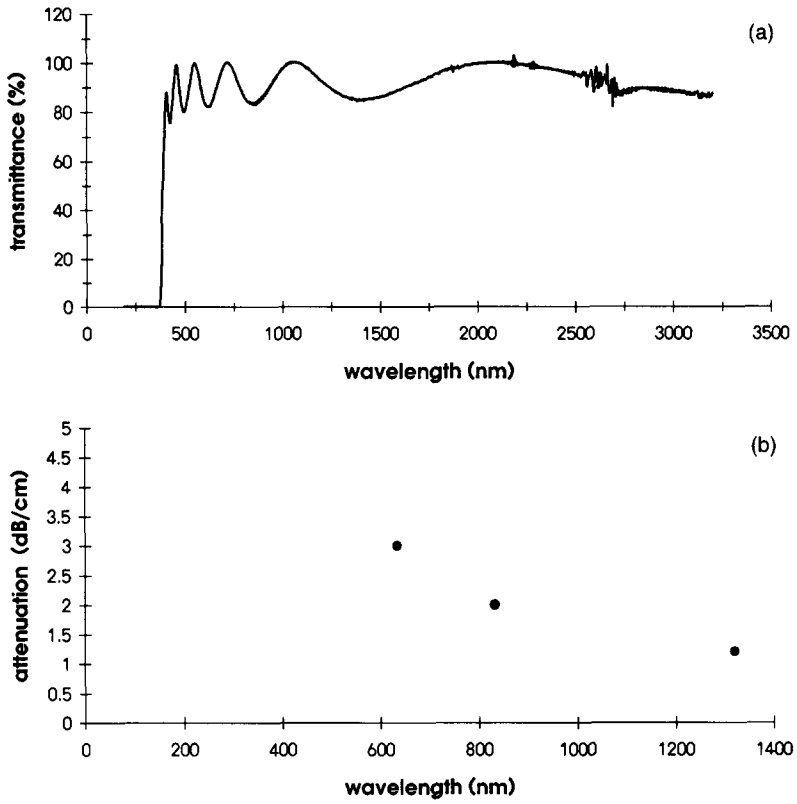

Fig. 2. Optical transmission spectrum of a ZnO type 1 film with thickness of 1/2 μm on a quartz substrate (a). Typical waveguide attenuation values of the lowest TE mode (TE_0) as a function of wavelength, with ZnO thickness of 1 μm (b).

tribution can be expected at a $d_{t\text{-}s}$ value of 3/4 of the plasma diameter (~5 cm). Nevertheless, this 3.5 cm value will not be used as the set-point, for two reasons. The first reason is shown in Fig. 1b. Here the thickness uniformity in the close proximity of this $d_{t\text{-}s}$ value is given, clearly showing the – too – large depence upon this distance, while also the circular thickness symmetry is disturbed (probably due to a plasma asymmetry, caused by the off-center inlet of the oxygen gas). The other reason is that this distance is too small to prevent the layer from electron bombardment. This bombardment results in a largely increased surface roughness and (probably) extra crystal defects, thereby dramatically increasing the waveguide losses for ZnO layer thicknesses larger than 1/2 μm. Therefore the 10 cm value will be used as the $d_{t\text{-}s}$ set-point value.

Table 1
Optimized ZnO process parameters for minimal attenuation values

	type 1	type 2
$d_{t\text{-}s}$ (mm)	100	100
P_{O_2} (Pa)	2	1/2
T_s (°C)	590	350–425
P_{RF} (W)	1800	1000

3.2. Optical characterization

With the $d_{t\text{-}s}$ value of 10 cm the other proces parameters were varied to minimize the waveguide attenuation. Besides waveguide thickness and film structure, this parameter is strongly dependent on the wavelength used. This is illustrated in Fig. 2a, where the optical transmittance measured with a beam perpendicular to the film surface in the range from 190 to 3200 nm is shown. The figure is corrected for the substrate transmittance. The ZnO film with thickness of 1/2 μm is deposited on a quartz substrate using the deposition parameters corresponding to "ZnO type 1" as shown in Table 1. Clearly visible is the ZnO absorbance edge at approximately 380 nm (bandgap energy ≅ 3.25 eV), while the thin film interference causes the intensity

modulations. The waveguide losses depend upon the wavelength used, not only because of this intrinsic absorbance of ZnO, but probably also because of wavelength-dependent scattering losses etc. This is shown in more detail in Fig. 2b, were typical attenuation values for a 1 μm thick ZnO (type 2 after post-deposition annealing, see next section) as a function of wavelength are shown. From this figure is can be concluded that ZnO is not suitable for waveguide applications beneath approximately 500 nm. Furthermore, it can be seen that the waveguide optical losses decrease with increasing wavelength: at $\lambda = 1.3$ μm the attenuation is typically 2 times lower than at 632.8 nm.

Attenuation and refractive index as a function of annealing

For comparison the waveguide attenuation measurements were done at one wavelength (632.8 nm) with a standardized thickness (1/2 and 1 μm) on a thermally oxidized (2 μm) Si-wafer. The 632.8 nm wavelength is selected because of its clear visibility and its sufficient distance from the bandgap region (see Fig. 2).

The characterization was done as a function of anneal time. The post deposition annealing was done in ambient atmosphere, because initial experiments in either O_2 and/or N_2 atmosphere revealed no significant difference (probably due to the non-100% purity of the gases used).

In contrast to previously reported investigations [8], we found *two* parameter sets in which the attenuation reaches a (local) minimal value, with largely different resulting optical parameters: one which requires a post-deposition anneal step (referred to as type 2 ZnO), and one which doesn't (type 1 ZnO). The corresponding process parameters are summarized in Table 1.

The resulting type 1 ZnO layers have attenuation values at wavelength of 632.8 nm which are ≈ 2 dB/cm, almost independent of the layer thickness, see Fig. 3.

The refractive index measurements at the same wavelength yield two indices, $n_{\parallel}$ (with TE-modes) and $n_{\perp}$ (with TM-modes). Their values, being measured at 5 positions at the wafer, are: $n_{\parallel} = 1.994 \pm 0.001$, $n_{\perp} = 2.009 \pm 0.001$ (errors due to irreproducibility included). Comparing these values with that of single crystal ZnO (1.9903 and 2.0065, respectively [15]) reveals that the films are properly oriented (poly)crystalline ZnO (see also Section 3.3). Therefore the $n_{\parallel}$ and the $n_{\perp}$ will be denoted as the ordinary (n_o) and extra-ordinary (n_e) refractive index, respectively.

Post deposition anneal steps hardly alter neither the attenuation nor the refractive indices, see Figs. 3 and 4, respectively. For convenience, the shown curves in these figures represent process parameters in the proximity of the optimized sets only. The most critical process parameter is T_s: lowering the substrate temperature below 500°C results in a less oriented structure (as measured with the prism coupling method via a strongly reduced difference between n_o and n_e) going with a dramatical increase in attenuation compared to the optimized situation.

For the type 2 ZnO layers the situation is completely different. The attenuation values are (at this wavelength) typically 1–3 dB/cm at $\frac{1}{2}$–1 μm, respectively. It should be noted however that these attenuation values cannot be obtained without post-deposition annealing, see Fig. 3. Before annealing the attenuation is very high ($\gg 100$ dB/cm). Interestingly, the anneal steps go with sharply reduced refractive indices, see Fig. 4. The limiting refractive index values are not as uniform over a wafer as is the case with situation 1: ± 0.005, while the reproducibility error has the same value: ± 0.005. The required minimal anneal temperature is 400°C: as already reported in literature [10], we found that the same results are obtained in case of a reduced required anneal time by increasing the anneal temperature to 450°C. Too long annealing at this temperature or increasing the temperature to 500°C or higher values leads to increased attenuation values, probably due to microfracturing.

In contrast to ZnO type 1, P_{O_2} rather than T_s is the critical parameter in ZnO type 2. The T_s value can be decreased to (at least) 125°C without sharply increasing the attenuation values, see Fig. 3b. It should be noted that the resulting refractive indices can be adjusted using the P_{RF} and the T_s value.

Both ZnO types show a slightly reduced difference between n_o and n_e with post-deposition annealing, typically from 0.020 to 0.015.

Refractive index dispersion

The transmittance curve shown in Fig. 2a corresponds with a typical (ordinary) refractive index behaviour shown in Fig. 5a. Here the dispersion curves

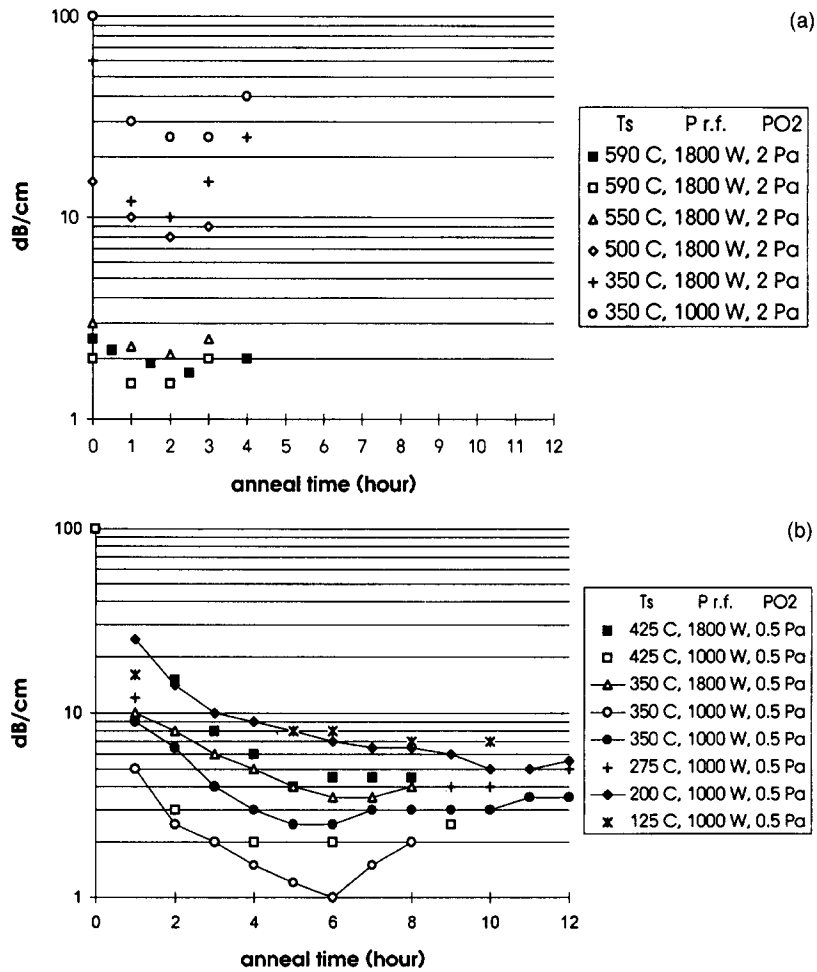

Fig. 3. TE_0-mode attenuation values (at wavelength of 632.8 nm) of type 1 (a) and type 2 (b) ZnO layers, as a function of anneal time at 450°C in ambient atmosphere. The experimental error (errors due to irreproducibility included) is $\pm 1/2$ dB/cm (not shown in the figures). The ZnO thickness is 1/2 μm (open markers) and 1 μm (filled markers). The process parameters substrate temperature T_s, r.f. power P_{RF} and oxygen pressure P_{O_2}, are used as parameter, while the distance between target and substrate $d_{t\text{-}s}$ is fixed at 100 mm.

of a 1/2 μm ZnO layer of type 1 and type 2 (before and after post-deposition annealing) are shown, using the prism coupling method at five different wavelengths. From this figure a substantial difference in dispersion becomes visible.

The refractive index dispersion data (below the band gap) can be fitted to the well known Sellmeyer approximation [17],

$$n^2 = A + \frac{S \cdot \lambda^2}{\lambda^2 - \lambda_0^2} \quad (\text{with } \lambda \text{ in nm}), \tag{1}$$

where n is the refractive index for a specified direction of light polarization, A represents a dispersionless background and S the oscillator strength of the absorption band with resonance wavelength λ_0. They can also be fitted to the simpler single-oscillator description [19,20],

$$n^2 - 1 = \frac{E_d \cdot E_0}{E_0^2 - E^2} \tag{2a}$$

or alternatively

$$\frac{1}{n^2 - 1} = \frac{E_0}{E_d} - \frac{h \cdot c}{E_0 \cdot E_d} \cdot \frac{1}{\lambda^2}, \tag{2b}$$

where E is the photon energy, E_0 is the energy of the effective dispersion oscillator (typically near the main peak in the absorption spectrum), and E_d is the so-called dispersion energy. The latter quantity is very

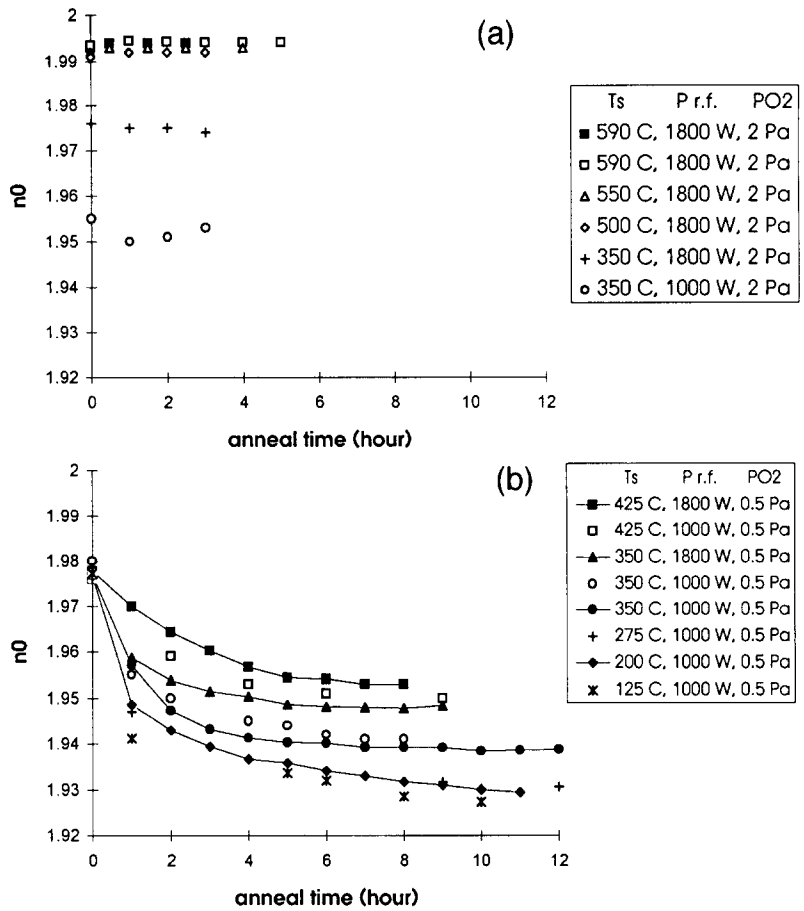

Fig. 4. Ordinary refractive indices (at wavelength of 632.8 nm) of the type 1 (a) and type 2 (b) ZnO layers, as a function of anneal time at 450°C in ambient atmosphere (the corresponding extra-ordinary refractive indices show the same behaviour and are therefore not shown). The ZnO thickness is 1/2 μm (open markers) and 1 μm (filled markers). The process parameters substrate temperature T_s, r.f. power P_{RF} and oxygen pressure P_{O_2}, are used as parameter, while the distance between target and substrate $d_{t\text{-}s}$ is fixed at 100 mm.

nearly independent of E_0 and provides an independent oscillator strength quantity which can be related to the packaging density of the crystal [20]. Therefore the single oscillator expression will be used, as this provides information which can be directly related to the crystal structure. In Fig. 5b a plot of the (ordinary) refractive index factor $(n_0^2-1)^{-1}$ versus λ^{-2} is shown. The filled markers correspond to the refractive index data for single crystal ZnO [15], while the straight line is the calculated curve using the single crystal values for E_0 and E_d (see Table 2) from literature [19]. At long wavelengths a positive curvature deviation from linearity is visible, due to the negative contribution of lattice vibrations to the refractive index, while at short wavelengths a negative curvature deviation occurs due to the proximity of the absorption band. The open markers in Fig. 5b represent the experimental data for the two ZnO types. From this plot E_0 and E_d values can be calculated.

In Table 2 the results are presented, when applied on the ordinary refractive index n_o. Because annealing has hardly any influence on type 1 ZnO, this type is represented by only one column. From the E_0-value the wavelength at which maximum absorption occurs ($\lambda_{abs.max.}$) is calculated.

From this table it follows that the values for ZnO type 1 agree well with those for a ZnO single crystal, in contrast to ZnO type 2.

In the next section we will further investigate the differences between the two optimized ZnO types by examining their structural characteristics. Most attention will be paid to the post-deposition anneal effects

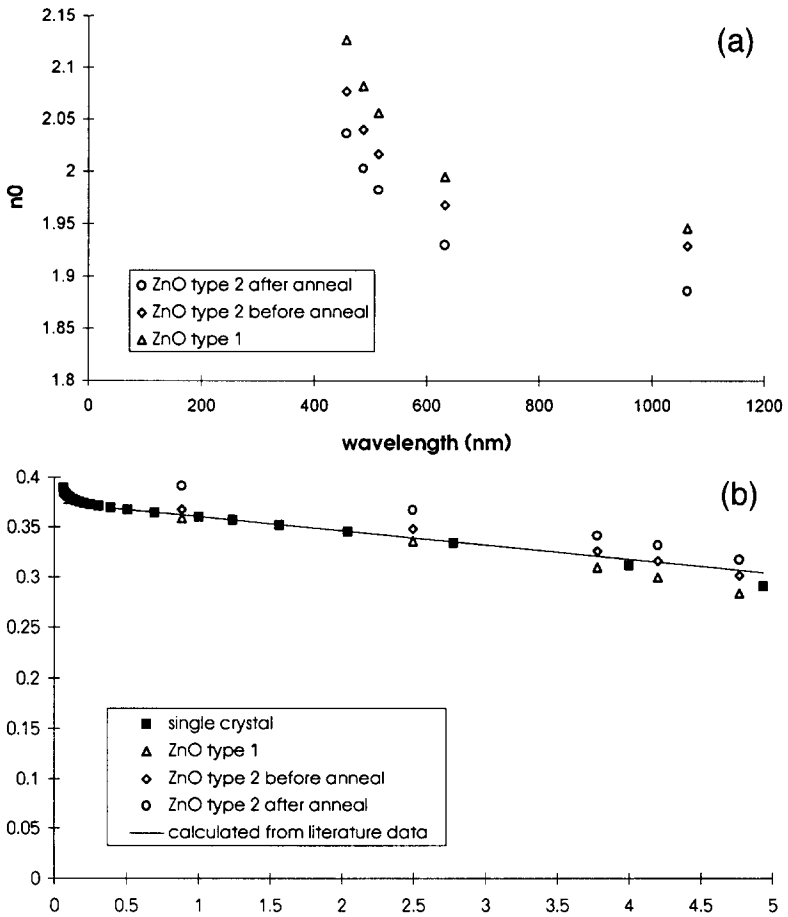

Fig. 5. Comparison of the ordinary refractive index dispersion curves of ZnO type 1 and those of ZnO type 2, before and after annealing (a). The shown dispersion data are measured using the prism coupling method using the wavelengths: $\lambda = 457.9, 488, 514.5, 632.8$ and 1064 nm. In (b) plots of the (ordinary) refractive index factor $(n_0^2 - 1)^{-1}$ versus λ^{-2} using the single-oscillator description are shown. The filled markers correspond to the refractive index data for single crystal ZnO [15]. The straight line is the calculated curve using the single crystal values for E_0 and E_d (see Table 2) from literature [19].

on the c-axis lattice constant, as this parameter is found to be closely correlated to the refractive index behaviour of the ZnO [16].

Table 2
E_0 and E_d constants describing the ordinary refractive index dispersion using the single-oscillator description

	ZnO single crystal theory (Ref. [19])	ZnO-type 1	ZnO-type 2	
			before anneal	after anneal
E_0 (eV)	6.4	6.4±0.1	7.0±0.1	6.5±0.1
$\lambda_{abs.max.}$ (nm)	194	195±3	180±3	191±3
E_d (eV)	17.1	17.2±0.3	18.5±0.3	16.2±0.3

3.3. Structural characterization

Crystallographic symmetry

Cystalline ZnO belongs to the wurtzite class of crystals (i.e. a hexagonal closest packed lattice). When deposited on substrates, it exhibits a strong tendency to grow with its c-axis perpendicular to the substrate [21]. In Fig. 6 a typical θ–2θ scan (of type 1 ZnO) and a typical rocking curve (of type 2 ZnO after post-deposition annealing) are shown. Because of its amorphous character, the thermally grown SiO_2 layer is not contributing any diffraction peak.

From the curves shown in Fig. 6 we immediately can draw the conclusion that – as expected – both ZnO

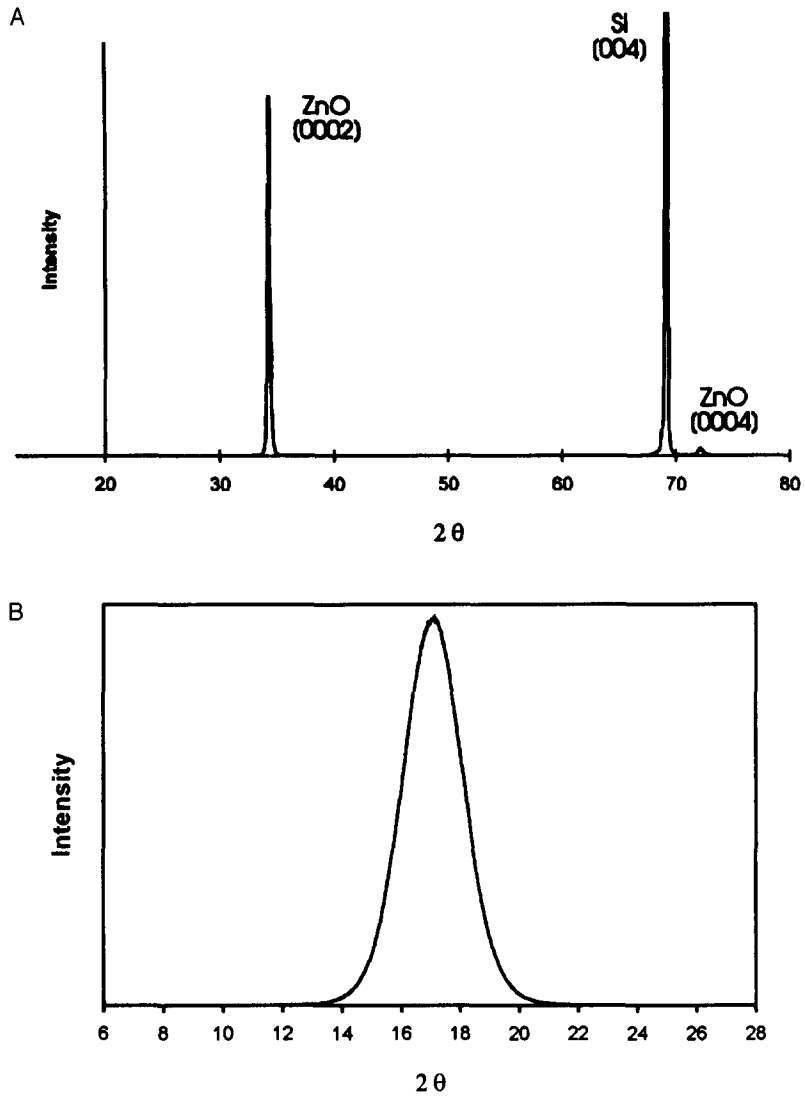

Fig. 6. Typical θ–2θ scan – of ZnO type 1 – (a) and rocking curve – of ZnO type 2, after post deposition annealing (b).

types are clearly crystalline, and indeed exhibit a preferential growth direction c.q. orientation of their c-axis perpendicular to the substrate. The latter follows from the absence of reflections other than the (0002) and the (0004) planes.

In Table 3 relevant data given by the XRD-measurements are presented.

From these data the following structural information can be derived.

c-axis lattice constant and residual (macro) strain

The exact position of the XRD-peaks and thus also the c-axis lattice constant and the macro strain value depend on the type of ZnO materials. The calculated values are presented in Table 4. The experimental errors in the data presented in Table 4 are less than 0.2%.

The difference in c-axis lattice constants has to be attributed to the occurrence of stresses in the films, all of them having the c-axis perpendicular to the substrate surface. Under compression (parallel to the surface), the c-axis lattice constant will increase, leading to a somewhat larger interplanar distance for the (0002) planes. Under tension the reverse occurs. All strains are possitive, which indicates that the films are stretched perpendicular to, and therefore compressed

Table 3
Typical XRD experimental results

	ZnO type 1		ZnO type 2	
	before aneal	after aneal	before anneal	after anneal
2θ (0002)	34.24°	34.26°	33.87°	34.27°
FWHM (0002)	0.266°	0.247°	0.710°	0.342°
2θ (0004)	72.13°	72.18°	71.38°	72.23°
FWHM (0004)	0.60°	0.58°	1.60°	0.75°
rocking curve FWHM (0002)	2.77°	2.46°	2.61°	2.37°

Table 4
Typical c-axis lattice constants and residual strain values. The single crystal value is 0.521 nm [16]

	ZnO type 1		ZnO type 2	
	before aneal	after aneal	before anneal	after anneal
c-axis lattice constant.	0.5238 nm	0.5232 nm	0.5288 nm	0.5232 nm
residual (macro) strain	0.60–0.65%	0.50–0.55%	1.50–1.60%	0.50–0.55%

Table 5
Typical micro-strain values

	ZnO type 1		ZnO type 2	
	before aneal	after aneal	before anneal	after anneal
micro strain	0.45–0.5%	0.5–0.6%	1.6–1.8%	0.7–0.9%

parallel to the film surface. The existence of a compression is confirmed by the nature of the curvature of the Si-wafers. Measuring this curvature by using a surface profiler (Sloan Dektak 3030) qualitatively confirms the results given in Table 4.

From this table we find that the literature value of the c-axis lattice constant for single crystals is never obtained. As expected from the refractive index data, type 1 ZnO, which resembles the single-crystal form, has a c-axis lattice constant which is hardly altered by the post-deposition annealing. On the other hand type 2 ZnO shows a large decrease in c-axis lattice constant with annealing. The latter is going with a sharp decrease in stress in the layers (see also section *micro-strain*).

Texture

As mentioned in Section 2.2 information about the film texture can be obtained from the rocking curves. From Table 3 it can be seen that before annealing there is only a small difference between the FWHM values of the two ZnO types. After the post-deposition annealing this mutual difference becomes even smaller. It can therefore be concluded that the spread in orientation from the ZnO columnar c-axis is approximately the same for both ZnO types: the FWHM value of $\cong 2.5°$ means that more than 68% of all the columns are oriented within 1° deviation from the c-axis. Interestingly, the post-deposition annealing leads to a significantly smaller rocking curve FHWM value, which probably corresponds to the (measured) small decrease in difference between the the refractive indices ($n_e - n_o$) for both ZnO types (see Section 3.2).

Micro-strain

From the broadening of the XRD-lines data can be obtained on the micro-strain values (e.g. local lattice distortions). Using Scherrer's relation, this phenomenon can be distinguished from other line broadening effects through its specific dependence upon the angle θ. In Table 5 the typical values are summarized.

From this table the same tendency can be observed as with the macro-strain, with one exception: ZnO type 1 shows a slight increase in microstrain with post-deposition annealing.

3.4. SEM and TEM microscopy

In Fig. 7 the SEM pictures of the cross-section of two typical ZnO layers are shown. Both layers have a thickness of 1/2 μm and are grown on a 2 μm thick SiO_2 layer on a Si-support (also the attenuation values are the same, appr. 2 dB/cm at 632.8 nm). Interestingly, the post-deposition annealing applied to both samples doesn't change the difference in the SEM images.

From these figures the columnar growth perpendicular to the substrate is clearly visible. The photographs also suggest that the columnar width is approximately the same for both ZnO types (typically 50 nm), which is not obvious [22] in view of the large difference in

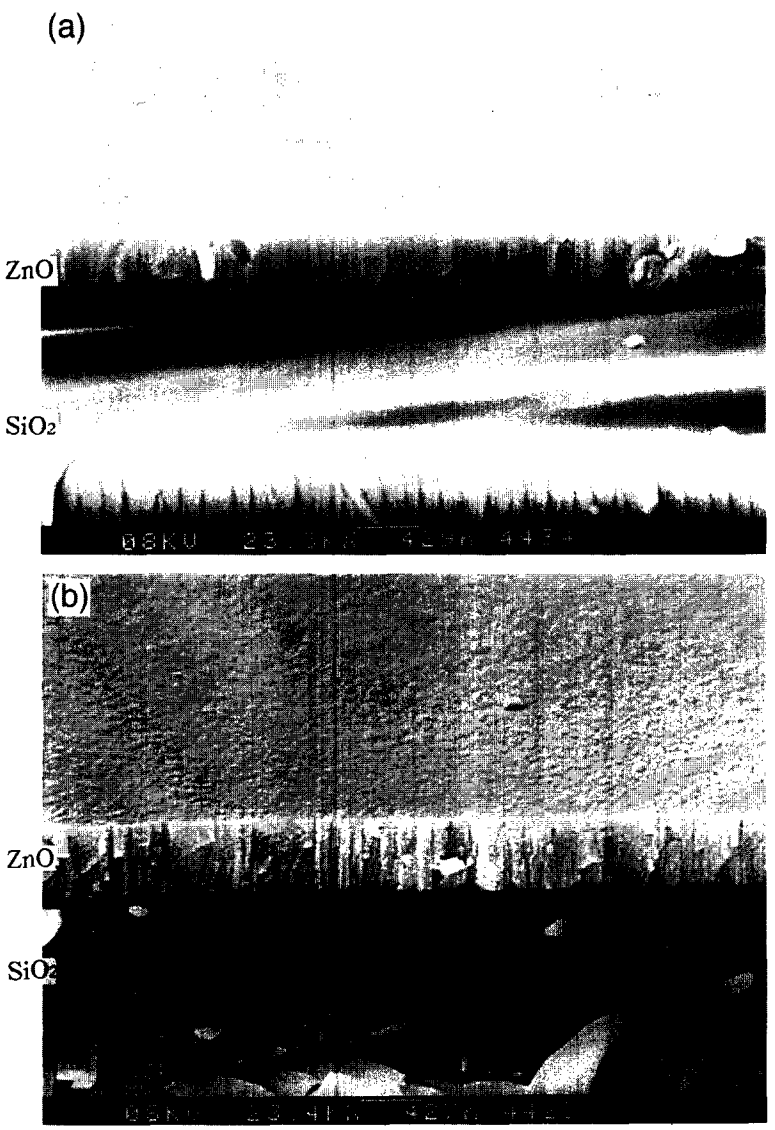

Fig. 7. Scanning electron photographs (SEM) of the cross section of thin films of ZnO type 1 (a) and ZnO type 2 (b) after post-deposition annealing. The ZnO layers have a thickness of 1/2 μm and are grown on 2 μm SiO_2.

substrate temperature and considering the resulting large optical differences. Furthermore, the columnar width seems to be more or less constant through the whole layer, without the presence of a (visible) initial layer. The latter is probably due to the limited resolution of the apparatus used. Most important feature however is the clear difference in package density between the two samples, with the ZnO type 1 (resembling the single crystal form) having the larger density.

In Fig. 8 typical bright field TEM pictures of the two ZnO types are shown. The ZnO type 1 layer shows sharp columnar boundaries, which are less pronounced in the ZnO type 2 layer. For both ZnO types the columnar width is approximately 50 nm, in agreement with the dimensions visible on the SEM pictures. In contrast to Fig. 8b also a perfect very fine grid structure with a period of $\cong 0.5$ nm is visible in Fig. 8a, which probably represents the the ZnO lattice structure. Both observations are in agreement with the difference in resemblence to the single crystal form as suggested in Section 3.

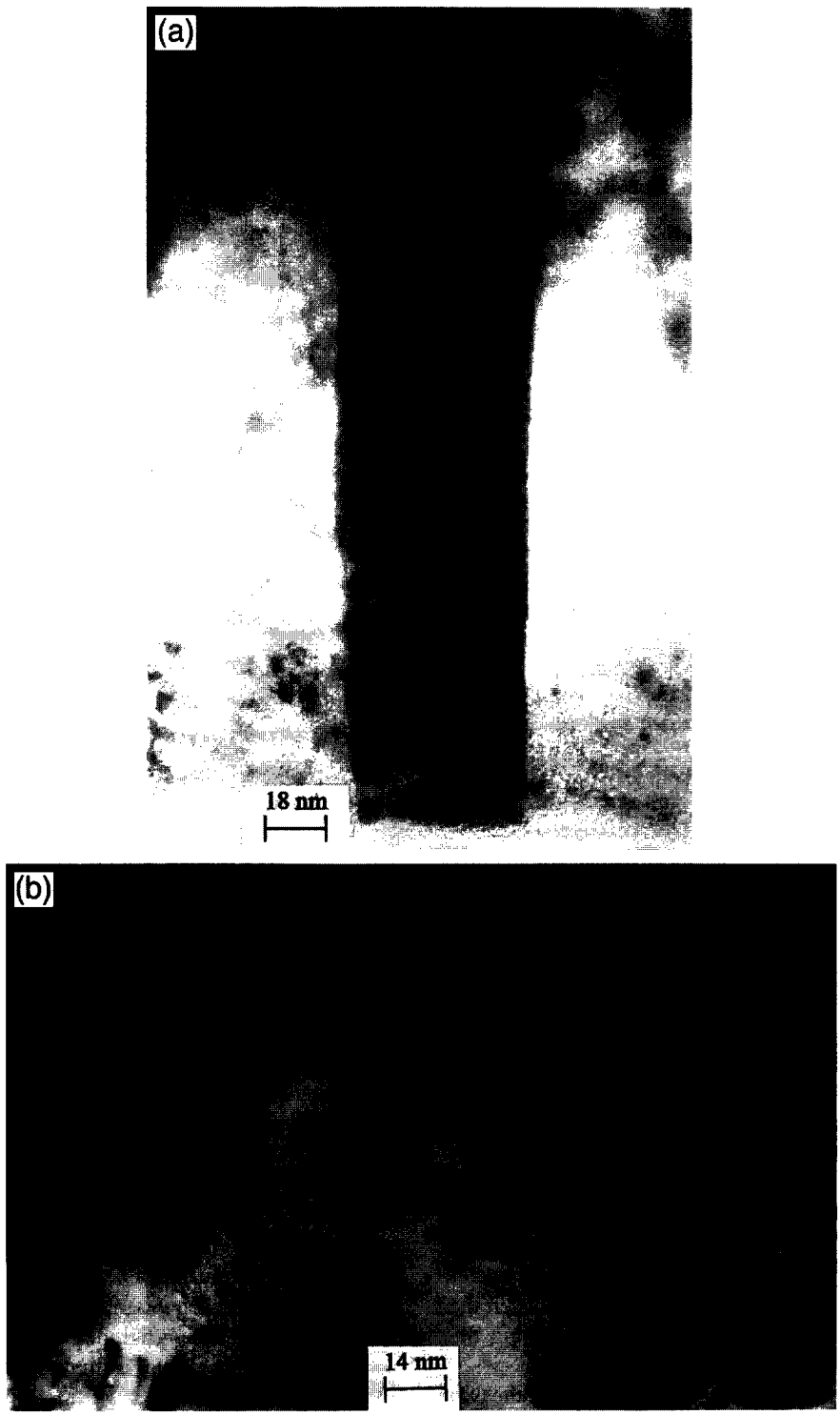

Fig. 8. Bright field transmission electron photographs (TEM) of ZnO type 1 (a) and of post-annealed ZnO type 2 (b)

3.5. Discussion

In Section 3.2. it was found that the two ZnO types both show relatively low waveguide optical losses (after annealing). From the XRD measurements we can conclude that both types correspond to layers which are clearly (poly) crystalline, with their c-axis oriented perpendicular to the substrate. This is confirmed by the measurements of the two refractive indices of the ZnO layers: the experimentally found difference for both types implies a specific crystal orientation. On the SEM and TEM photographs the crystal columns are clearly visible, with a width of approximately 50 nm for both ZnO types: the columnar width seems to be constant through the layer.

From the refractive index dispersion measurements it was concluded that ZnO type 1 resembles the single crystal form. Furthermore, these layers show negligable post-deposition anneal effects on refractive index and waveguide losses. With the XRD measurements it was found that also the structural properties show negligable post-deposition anneal effects. On the SEM photographs ZnO type 1 shows a densily packed crystal structure.

The ZnO type 2 shows a significantly different optical and structural behaviour, strongly depending upon the post-deposition anneal process. The deviating E_0 and E_d values of type 2 ZnO before annealing are found to correspond with a significantly different c-axis lattice constant. After post-deposition annealing, which largely reduces the c-axis lattice constant and (compressive) stress, it has its absorption peak maximum at the same wavelength as ZnO type 1 and single crystal ZnO. We suggest that the smaller $\lambda_{abs.max.}$-value (and therefore higher E_0-value, see Section 3.2) before annealing can be explained by excess Zn atoms in the layer. The post-deposition annealing process is then thought to oxidize the excess Zn atoms. This oxidation explains the sharply decreasing waveguide attenuation values and could be the origin of the observed correlation between light propagation loss and the value of the c-axis lattice constant which is also found in literature [18]. Furthermore, it explains the decreasing refractive indices and the shifting $\lambda_{abs.max.}$. It also explains the experimentally observed decreasing conductivity (several orders of magnitude), which will be discussed in another paper.

After post-deposition annealing ZnO type 2 shows a significantly lower E_d value than those of single crystal ZnO and ZnO type 1, while the E_0 value and the c-axis lattice constants are identical. This can be explained by a difference in package density of the crystal columns [20], which indeed is clearly visible in the SEM pictures. The observed structural characteristics also correspond to this difference in package density: a low columnar crystal package density, as suggested for the type 2 ZnO, enables the observed large variation in lateral (compressive) stress. It can therefore be concluded that the significant difference between the refractive indices of the two ZnO types is caused by a difference in package density of the crystal columns.

4. Applications

One application was already mentioned in Section 1. Using the difference in refractive index of the two ZnO types, sandwich (channel) waveguides can be formed with an optical mode profile resembling that of a standard single mode fiber (see Fig. 9a). In this figure the channel is fabricated in the waveguiding layer (ZnO type 1): this can be achieved using ion beam etching (IBE). To obtain even smaller refractive index differences, it is also possible to use the adjustability of the

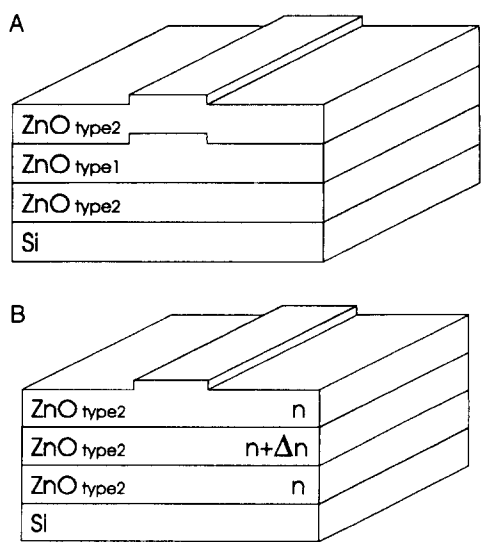

Fig. 9. ZnO sandwich structures forming optical waveguides. In (a) both ZnO types are used, with channel definition in the waveguiding (ZnO type 1) layer. In (b) a waveguide structure formed by ZnO type 2 only is shown, with channel definition in the cover layer.

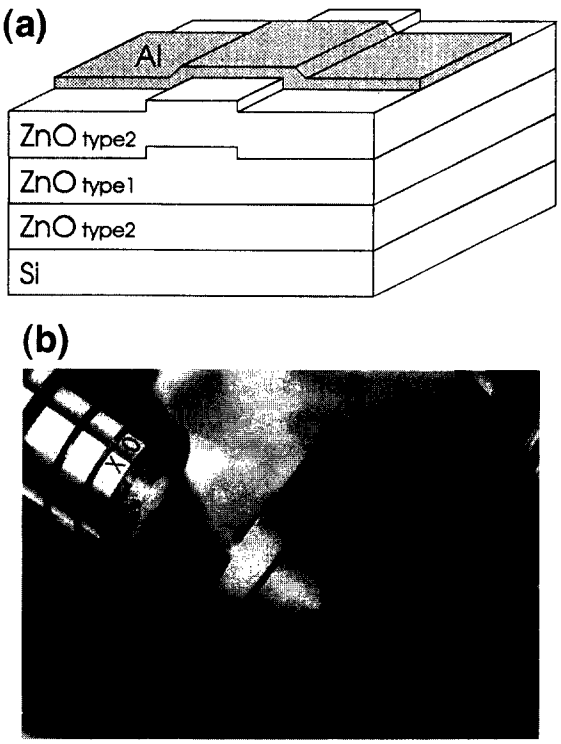

Fig. 10. Optical waveguide configuration combining the two ZnO types, yielding environmental shielding (a). In (b) a photograph is shown of the propagation of light (wavelength 632.8 nm) through such a waveguide structure.

low refractive index ZnO type 2 (see Fig. 9b). The index profile can even be graded by adjusting the substrate temperature during deposition. For convenience, the channel definition is now done in the cover region.

Another application is found in the acousto-optical field. In the waveguide structure shown in Fig. 9a metal electrodes can be deposited on top of the structure without any increase of the optical attenuation (see Fig. 10a). This offers three major advantages. First, the complete waveguide structure is made of ZnO, resulting in larger electro-optical effects. Secondly, the ZnO layer combination, being much thicker than the optical waveguiding layer itself, can act as the acoustical waveguide. This enables a much more efficient exitation [23]. Finally, the acoustical waves can be generated at the applied waveguide directly.

In Fig. 10b a photograph is shown, showing the environmental shielding property of a such a waveguide configuration. For convenience, the substrate layer of ZnO type 2 is replaced by thermally grown SiO_2. The aluminium stripes have a width of 1 mm and a thickness of 200 nm.

5. Conclusions

In these experiments we have shown that thin (~ 1 μm) crystalline ZnO films with a good optical quality and a good (0002) texture can be grown under considerably different process parameters. The ZnO deposition procedure was optimized with regard to two boundary conditions stemming from the IO application, e.g. low optical losses and good thickness uniformity. The optical parameters of the corresponding ZnO layers are distinctly different. Besides a high refractive index ZnO film resembling the single crystal form, also ZnO films with considerably lower refractive indices (typical difference 0.05) can be produced. The refractive index of the latter ZnO type is adjustable (~ 1.93–1.96 at $\lambda = 632.8$ nm) through the process deposition parameters.

The optical waveguide losses for both ZnO types are typically 1–3 dB/cm at a wavelength of 632.8 nm. In contrast to the high refractive index ZnO films, the low refractive index ZnO layers need a post deposition annealing step however to reach these attenuation values. This is probably needed to oxidize excess zinc in the films. This post-deposition annealing not only decreases the waveguide optical losses and the refractive index of the low refractive index ZnO, but also results in reduced micro- and macro strain values. Furthermore, the c-axis latice constant value is sharply decreased.

Most of the crystallographic parameters as measured with XRD after the post-deposition anneal step are approximately the same for the two ZnO types: c-axis lattice constant ($\cong 0.5235$ nm), residual strain ($\cong 0.5\%$) and rocking curve FWHM ($\cong 2.4°$). Only the microstrain values are slightly different: 0.5–0.6% (ZnO type 1) and 0.7–0.9% (ZnO type 2). The difference in refractive index dispersion between the two ZnO types is most probably caused by a difference in package density of the crystal columns. This can indeed be seen on the SEM pictures of the two different ZnO types.

The two ZnO types are used to fabricate optical channel-and slab waveguides with small refractive index differences, the core and the cladding both showing the

desired electro-optical and piezo-electrical behaviour. With this configuration metal electrodes can be fabricated directly on top of the waveguide structure without any increase of the optical attenuation. Furthermore the fabrication of channel waveguides with mode characteristics resembling the field distributions of standard optical fibers is now possible, enabling a largely improved fiber-to-chip coupling efficiency.

Acknowledgements

These investigations were supported by the Dutch Innovative Research Program (IOP) Electro-Optics.

The authors want to thank A.M. Otter (MESA Research Institute) for the SEM photographs and Dr. E.G. Keim (Center for Materials Research) for the TEM photographs.

References

[1] S. Ono, K. Kiyotaka and S. Hayakawa, Wave Electronics 3 (1977) 35.
[2] T. Mitsuyu, O. Yamazaki, K. Ohji and K. Wasa, Ferroelectrics 42 (1982) 233.
[3] F.R. Blom, D.J. Yntema, F.C.M. van de Pol, M. Elwenspoek, J.H.J. Fluitman and Th.J.A. Popma, Sensors and Actuators A21–A23 (1990) 226.
[4] C.J. vam Mullem, F.R. Blom, J.H.J. Fluitman and M. Elwenspoek, Sensors and Actuators A25–27 (1991) 379.
[5] H. Herrmann, K. Schäfer and W. Sohler, IEEE Photonics Technology Lett. 6 (1994) 1335.
[6] W. Warzanskyj, F. Heismann and R.C. Alferness, Appl. Phys. Lett. 53 (1988) 13.
[7] F.S. Hickernell, Digest of the Topical Meeting on Integrated and Guided Wave Optics, WB6-1 (1980).
[8] W.H.G. Horsthuis, Thin Solid Films 137 (1986) 185.
[9] S. Dutta and H.E. Jackson, Appl. Phys. Lett. 39 (1981) 206.
[10] H.H.P.Th. Bekman, K.W. Benoit and J.L. Joppe, Applied Surface Science 70/71 (1992) 347.
[11] F.C.M. van de Pol, Ph.D. thesis, University of Twente (1989).
[12] R. Ulrich and R. Torge, Appl. Optics 12 (1973) 2901.
[13] S. Miganaga, M. Imai and T. Asahura, IEEE J. Quantum Electon. QE-14 (1978) 30.
[14] S.B. Krupanidhi and M. Sayer, J. Appl. Phys. 56 (1984) 3308.
[15] W.L. Bond, J. Appl. Phys. 36 (1965) 1674.
[16] Handbook of Chemistry and Physics (CRC press, Cleveland, 1963).
[17] K. Clays, N.J. Armstrong and T.L. Penner, J. Opt. Soc. Am. B. 10 (1993) 886.
[18] S. Takada, J. Appl. Phys. 73 (1993) 4793.
[19] S.H. Wemple and M. DiDomenico, Phys. Rev. B 3 (1971) 1338.
[20] S.H. Wemple, Phys. Rev. B 7 (1973) 3767.
[21] T.L. Tansley, D.F. Neely and C.P. Foley, Thin Solid Films 117 (1984) 19.
[22] H.H. Afify, S.A. Nasser and S.E. Demian, J.Mat.Sci.: materials in electronics 2 (1991) 152.
[23] F.S. Hickernell, J. Appl. Phys. 44 (1973) 1061.